Hindawi Publishing Corporation
Journal of Nanomaterials
Volume 2012, Article ID 327369, 14 pages
doi:10.1155/2012/327369

Research Article

Morphological Characterization of Nanofibers: Methods and Application in Practice

Jakub Širc,[1] Radka Hobzová,[1] Nina Kostina,[1] Marcela Munzarová,[2] Martina Juklíčková,[2] Miloslav Lhotka,[3] Šárka Kubinová,[4] Alena Zajícová,[5] and Jiří Michálek[1]

[1] *Institute of Macromolecular Chemistry, Academy of Sciences of the Czech Republic, Heyrovsky Square 2, 162 06 Prague 6, Czech Republic*
[2] *Elmarco, Ltd., V horkách 76, 46007 Liberec, Czech Republic*
[3] *Institute of Chemical Technology, Technická 5, 166 28 Prague 6, Czech Republic*
[4] *Institute of Experimental Medicine, Academy of Sciences of the Czech Republic, Vídeňská 1083, 142 20 Prague 4, Czech Republic*
[5] *Institute of Molecular Genetics, Academy of Sciences of the Czech Republic, Vídeňská 1083, 142 20 Prague 4, Czech Republic*

Correspondence should be addressed to Jakub Širc, sirc@imc.cas.cz

Received 31 May 2012; Accepted 18 September 2012

Academic Editor: Cheng Wang

Biomedical applications such as wound dressing for skin regeneration, stem cell transplantation, or drug delivery require special demands on the three-dimensional porous scaffolds. Besides the biocompatibility and mechanical properties, the morphology is the most important attribute of the scaffold. Specific surface area, volume, and size of the pores have considerable effect on cell adhesion, growth, and proliferation. In the case of incorporated biologically active substances, their release is also influenced by the internal structure of nanofibers. Although many scientific papers are focused on the preparation of nanofibers and evaluation of biological tests, the morphological characterization was described just briefly as service methods. The aim of this paper is to summarize the methods applicable for morphological characterization of nanofibers and supplement it by the results of our research. Needleless electrospinning technique was used to prepare nanofibers from polylactide, poly(ε-caprolactone), gelatin, and polyamide. Scanning electron microscopy was used to evaluate the fiber diameters and to reveal eventual artifacts in the nanofibrous structure. Nitrogen adsorption/desorption measurements were employed to measure the specific surface areas. Mercury porosimetry was used to determine total porosities and compare pore size distributions of the prepared samples.

1. Introduction

Nanofibers are currently one of the most intensively studied materials for applications in biomedical areas [1]. They have been employed as carriers for cell cultivation [2, 3], scaffolds in wound dressings [4], drug delivery systems [5], or for enzyme immobilization [6]. Internal architecture of nanofibrous materials is an important attribute which predisposes them as supporting materials in cell therapy, which is an attractive approach for the treatment of various diseases including chronic wounds [7] and corneal defects [8]. As carriers for cell cultivation, the role of the scaffold is to support "seeded" cells before *in vivo* transplantation. Therefore, the scaffold requirements include biocompatibility, controlled porosity and permeability and suitable mechanical properties comparable to natural tissue.

Various processing techniques have been used to produce nanofibers, such as drawing out [9], molecular self-assembly [10], or thermally induced phase separation [11]. However, the electrospinning technique [11–14] is the only one that allows the production of continuous polymeric nanofibers and provides numerous opportunities to manipulate and control surface area, fiber diameter, the porosity of the nanofibrous layer (fiber density) as well as basis weight (fiber weight per area). Electrospinning is a fiber spinning technique driven by a high voltage electrostatic field applied on a polymer solution that produces polymer fibers with diameters ranging from tens of nanometers to several micrometers. Modifications of a standard electrospinning

process, such as coaxial nanofiber preparation [15–17] or side-by-side nanofiber deposition, allow the formation of atypical nanofiber structures, for example production of nanocoils or nanosprings [18, 19]. Several methods have been described for the large scale production of nanofibers through an electrospinning process based on less productive needle or capillary spinners [20] (multiply nozzle blocks or needles [21]). However, these techniques have some disadvantages: low efficacy of the process regardless of the number of nozzles, poor nozzle cleaning, or discontinuity of electrospinning process. Unique needleless technology was used for nanofiber production, in which polymeric jets are spontaneously created from liquid surfaces [22, 23]. This is a completely original method of producing fibers in diameter of tens of nanometers to tens of micrometers. The needleless technology is very flexible and enables the creation of nanofibrous material from various polymers. The process provides very high production capacity, stability, and easy maintenance compared to other known "industrial scale" nozzle or needle technologies. With appropriate control of the process parameters, such as concentration of polymer in solution, electric field strength, tip-to-collector distance, or temperature, it is possible to prepare nanofibers of required structure from various polymers [24, 25].

Nanofibers despite its boom in recent years still represent a relatively new class of materials and it is desirable to consider not only the possibility of their preparation and applications but also their detailed characterization. Various features of nanofibers have been characterized, such as chemical composition [26, 27], mechanical properties [28–32], thermal behavior [29, 30, 32], or hydrophilicity/hydrophobicity [33–36]. Beside these properties morphology plays a key role in potential applications of nanofibers, especially in biomedical field [1, 25, 37]. The specific structure of nanofibers, however, necessitates a complex approach to examine the morphology using a combination of several methods. Unfortunately, most of the papers describe the structural parameters of nanofibers just briefly as a part of service methods. Only few reports are focused on theoretical approach to calculate for example, fiber diameter, sample thickness, or its porosity [19, 38–40].

The aim of this paper is to present readers a comprehensive overview of methods applicable for characterization of nanofibers, such as imaging methods, mercury porosimetry, or adsorption/desorption measurements, together with theoretical basis, advantages, and limitation of each method. This review part is supplemented by results of our research work done on morphological characterization of several types of nanofibers prepared by needleless electrospinning process. The structure and values of parameters such as fiber diameter, specific surface area, or porosity obtained by various methods are discussed.

2. Part 1—Review: Methods for Nanofiber Characterization

2.1. Imaging Methods. Imaging methods are nowadays widely used for evaluation of the structure and represent an essential part of characterization of the most materials, including nanofibers. The group of imaging methods involves particularly optical microscopy in the visible range, scanning electron microscopy (SEM), transmission electron microscopy (TEM), and atomic force microscopy (AFM). A great advantage of imaging methods is that the structure can be directly visualized at various places of the nanofibrous sample. Therefore, the obtained images provide the useful information to compare the local structures within the whole sample. Imaging methods also play a key role in the evaluation of *in vitro* biomedical experiments, depicting the cell cultivation process on various synthetic substrates. Despite the above-mentioned benefits, imaging techniques however do not provide defined numerical values to allow a quantitative comparison among various nanofibrous materials.

2.1.1. Optical Microscopy. Optical (light) microscopy has a number of advantages: the sample preparation is simple and the instrumentation is relatively cheap. The imaging takes place under the atmospheric pressure and the samples do not need to be dried. Therefore, the polymer samples can be monitored even in the swollen state, the same as they appear *in vitro* and *in vivo* experiments. Together with digitization of the signal, optical microscopy permits the monitoring of the changes of polymer sample structures during swelling or drying. These aspects predetermine the use of optical microscopy in bioapplications, where it is desirable to monitor all processes in physiological (aqueous) environment.

Unfortunately, limiting resolution of optical microscopy is about 200 nm which practically precludes this technique from characterization of nanostructures in detail. Optical microscope is used for preliminary examinations of nanofibrous materials during manufacturing process [41] or as a supporting part in apparatus for other more sophisticated methods (e.g., AFM).

Optical microscopy apparatus connected with high speed camera obtaining 2000 pictures/minute has been employed by Reneker et al. [42] to observe the processes on the top of the jet during electrospinning (Figure 1). The influence of various conditions on electrospinning of poly(ε-caprolactone), effect of mechanical and repulsive forces on the bending of the arising fiber and its consequent shape and formation has been explored.

2.1.2. Electron Microscopy. The output of electron microscopy is a result of the interaction of the sample with electron beam. Many factors such as electron energy, sample density, atomic number of elements and, obviously, topography of the sample surface, have an effect on this interaction. Elastic and nonelastic interactions of electrons with the sample atoms generate secondary electrons, Auger and backscattered electrons, continuum and characteristic X-rays and fluorescence. Usually, the secondary electrons are used for the SEM purpose, other products can also bring important information about the sample and they are used in other spectroscopic techniques.

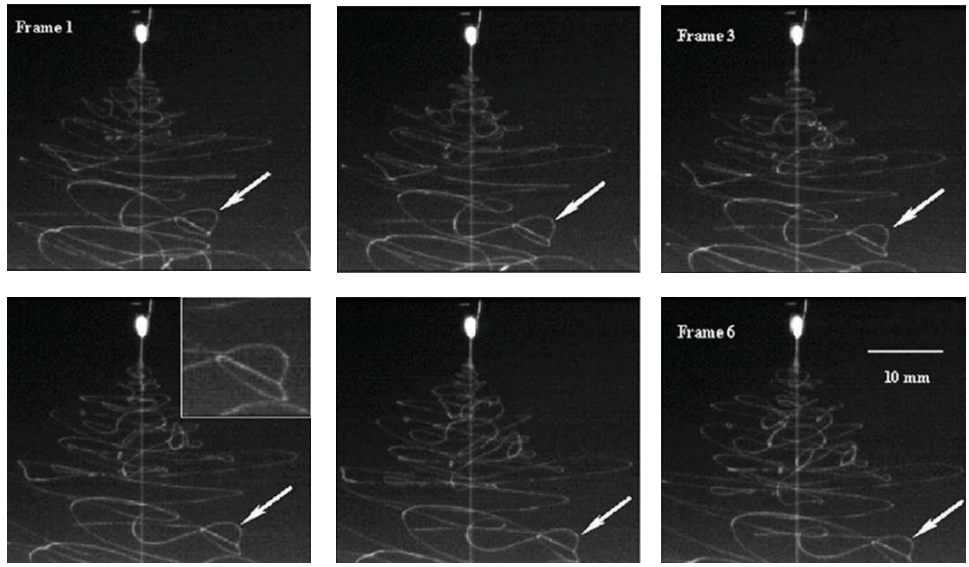

Figure 1: The loops formed during electrospinning of poly(ε-caprolactone) depicted by optical imaging apparatus connected with camera scanning at 500 frames/second [42].

To avoid a repulsive reaction of electron beam, the sample surface is usually covered with a thin layer of gold. Limitation of SEM is that the experiment proceeds under vacuum. During the sample drying, the crucial changes in the structure can appear. This aspect represents a drawback, especially in medicinal applications where polymer materials often swell in water environment. This disadvantage is partly solved in various modifications of SEM, such as low-vacuum scanning electron microscopy (LVSEM). This method works with a two-chamber system where the first high-vacuum detecting chamber is separated from the second low-vacuum one. Although the magnification is lower compared with standard SEM, it is not necessary to cover the sample surface with conductive layer. Environmental scanning electron microscopy (ESEM) and AquaSEM techniques proceed under the aqueous conditions and enable the observation of samples in wet state.

Generally, the benefit of SEM is high depth of sharpness providing information about structures at various distances from the scanning level, but on the other hand, it makes difficult simple measurement of the distance of two objects in the 2D depiction.

As mentioned above, imaging techniques allow direct visualization of the observed nanostructures. From this point of view, SEM is the useful method to evaluate the basic characteristics of prepared nanofibers (such as fiber diameter) and moreover, it enables to reveal artifacts in the nanofibrous structures arising during electrospinning under particular polymer concentration and conductivity of the electrospun solution [43]. The dependence of the conditions of electrospinning on fiber diameter was investigated by Amiraliyan et al. [41, 44]. By measuring diameters of 100 fibers of each sample they calculated distribution curves and compared the samples prepared under various conditions, such as temperature, electric field, or polymer concentration. With SEM, the authors found flat and ribbon-like character of the fibers in cross section and explained such origin in context of set jet parameters during electrospinning. Highly sophisticated methodology of the determination of fiber diameter as well as interfiber pore characteristics was described by Tomba et al. [45, 46]. Using mathematical algorithms for image analysis they highly improved predictive value of common SEM images. Fiber diameter distributions obtained by various methodologies are shown on Figure 2.

SEM and transmission electron microscopy (TEM) were found to be essential for investigation of nanofibrous materials with advanced structures, for example, core-shell structure obtained by coaxial electrospinning. As examples it can be mentioned as follows: (1) the nanocoil structures formed during side-by-side and off-centered coaxial electrospinning (Figure 3) and the influence of electrospinning conditions on the formation of such structures were investigated by Chen et al. [18, 19], (2) the structure of coaxial nanofibers prepared from collagen (shell) and polyurethane (core) was described [26], (3) so-called Janus morphology of side-by-side nanofibers prepared from two phases—polyvinylpyrrolidone and polyvinylpyrrolidone/polypyrrole was mentioned [27], or (4) detailed images of nanofibers prepared from poly(vinyl alcohol) of various molecular weight and montmorillonite were reported (Figure 4) [32, 47].

An interesting result brought experiments based on SEM imaging and testing of mechanical properties of natural ramie fibers reinforced with polyurethane (PUR) nanofibers. Images observed orientation and interconnection of fibers before and after application of strain on the ramie-PUR nanofibers and helped to understand the processes during tensile deformation [31].

SEM is also an irreplaceable method for evaluation of the nanofiber orientation, which not only affects the mechanical

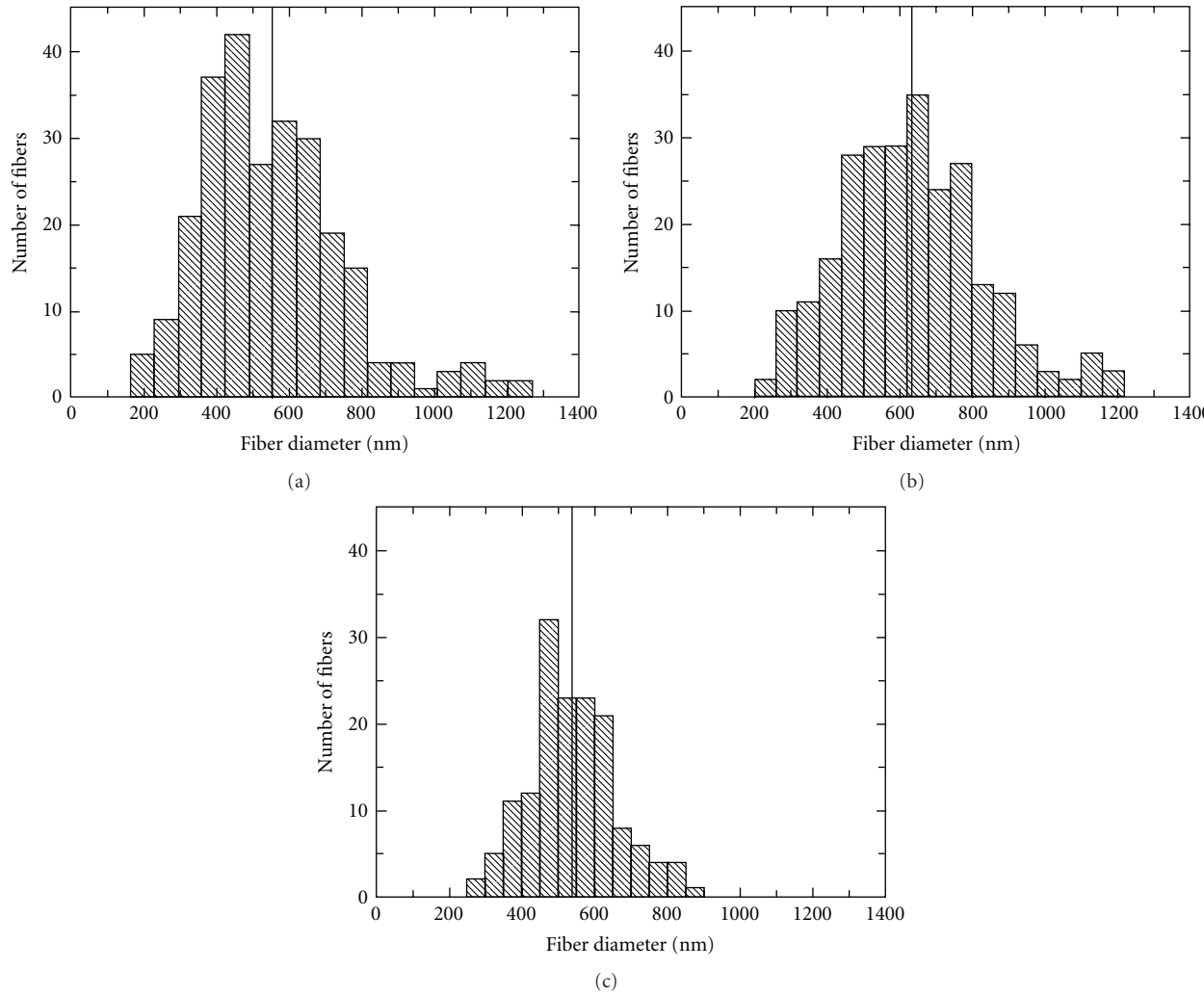

Figure 2: Fiber diameter distribution of nanofibrous membrane: (a) without considering perspective effects, (b) after considering perspective effects, (c) from manual measurement from the image. The vertical line in each diagram represents the distribution mean [45].

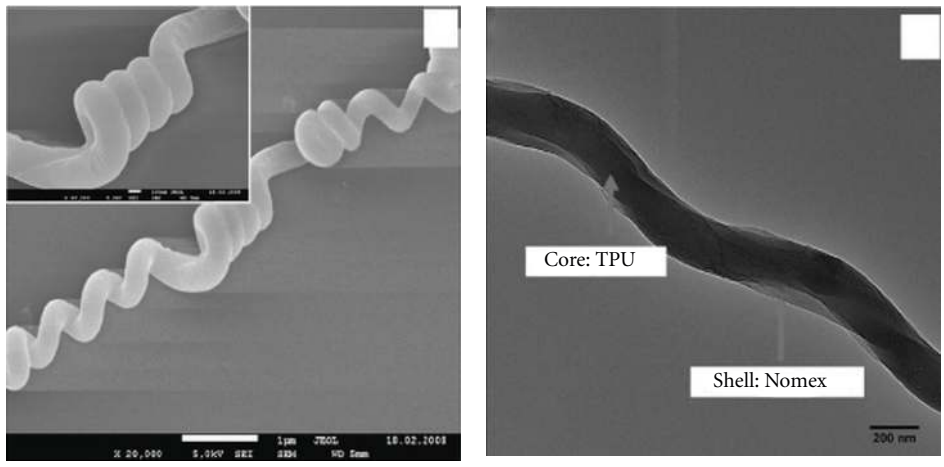

Figure 3: SEM (a) and TEM (b) images of polyurethane/Nomex nanocoils and core-shell nanofibers prepared by coaxial electrospinning [18].

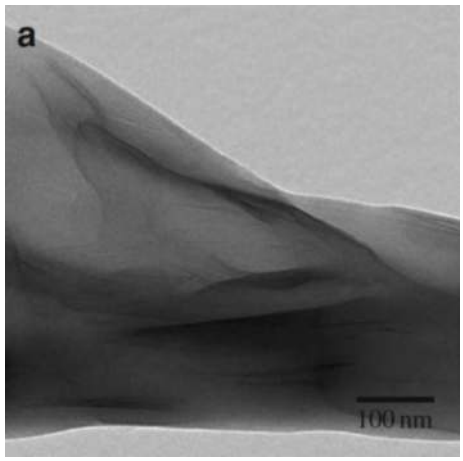

Figure 4: TEM images of nanofibers prepared from poly(vinyl alcohol) and montmorillonite [47].

properties [28, 48, 49] but also mainly plays a key role in the biological applications. Results obtained from *in vivo* and *in vitro* experiments showed significantly different behavior in dependence on either random or aligned arrangement of the fibers [50].

2.1.3. Atomic Force Microscopy. In atomic force microscopy, the surface of the sample is detected with the tip, moving in close proximity of the sample. The three-dimensional model of sample surface is reconstructed from individual positions of the tip. Characteristic is a high resolution, which in some applications can reach the atomic structure of crystals.

An important results can AFM bring in the examination of nanofibrous polymeric materials for medicinal applications—the structure of particular nanofibers can be observed [26] as well as fiber diameter can be effectively measured (Figure 5) [42]. Compared to electron microscopy techniques, AFM can operate in nonvacuum environment or in wet condition. Behavior of nanofibers in water or various organic solvents was observed by Stachewicz and Barber [51]. An interesting application of AFM was published [52], where AFM cantilever with tip was used as a nanomanipulator for investigation of mechanical properties of a single nanofiber. Although this technique requires sophisticated apparatus and skilled handling, more articles focused on AFM characterization of polymer nanofibers can be expected in the future.

2.2. Mercury Porosimetry. The method, invented in 1945 by Ritter and Drake [53], is based on the property of mercury that does not wet the surface of solid materials. During the measurement, the sample is placed in an evacuated cell, and mercury is then transferred into the sample cell under vacuum. Subsequently the pressure is applied to force mercury to penetrate to the pores of the sample. During the measurement, the applied pressure and intruded volume of mercury are recorded. As a result, an intrusion-extrusion curve is obtained. The parameters describing the pore structure of the sample can be calculated from the data.

With the approximation that all pores are of cylindrical shape, the Washburn equation (1) was deduced [54].

$$pr = -2\gamma \cos\Theta, \tag{1}$$

where p is the applied pressure, r is pore radius, Θ is the contact angle of mercury on the surface of solid sample, and γ is the surface tension of mercury. The contact angle between mercury and porous solid material varies somewhat with solid composition (from 112° to 142°). A value of 130° is recommended in the absence of specific information.

The Equation (1) is based on a simplified principle; however, real measurements are considerably influenced by many other factors. The penetration of mercury into the sample pores is a process which is affected by the size, quantity and shape of the pores, but also by the size of the sample. During the measurement, the adjusted rate of pressure increase is important; the time of attaining equilibrium is observed. The first part of an intrusion-extrusion curve depicts the pressure increase. With increasing pressure mercury gradually penetrates into smaller pores of the sample. At the limiting pressure 1000 MPa, mercury penetrates into the 2 nm pores. The second part of the curve depicts extrusion of mercury from the sample. The amount of mercury that remains in the pores predicts the pore character.

According to the shape of the intrusion-extrusion curve several pore shapes can be distinguished as follows.

(a) Cylindrical pores are characterised by a rapid penetration part of the curve. The extrusion part has a similar shape to the intrusion one. A negligible amount of intruded mercury remains in the pores.

(b) The penetration curve obtained for conical pores shows a slow increase caused by gradually decreasing pore diameter. Again, the extrusion curve follows the intrusion one. Conical pores are the most common in materials of natural origin.

(c) Slot pores having a shape of the space between two parallel plates are typical by a rapid increase of intrusion curve at higher pressures. A large amount of mercury remains in the pores after extrusion.

(d) Ink-bottle pores have narrow entrance to the wider internal space. After the extrusion almost all mercury remains in the pores.

The sample porosity is calculated from the mass of mercury intruded to the pores at the highest pressure. Using the mathematic apparatus corresponding to the particular shape of the pores (cylindrical, conical, slot, or ink-bottle), the specific surface area can be estimated from the total pore volume and pore diameters. For example, for pores of conical shape the surface is different than for the pores of the same size and volume but with a different shape. From a comparison of the estimated surface area with the result of exact measurement by BET technique (see below), the predominant pore shape can be found.

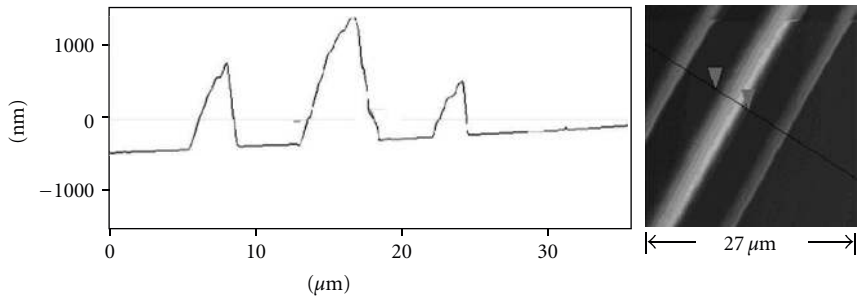

Figure 5: Diameters of three polycaprolactone nanofibers measured by atomic force microscopy. The diameter was measured from the baseline to the maximum height of the peak to eliminate errors from the shape of the tip [42].

The most often presented result of mercury porosimetry is a pore size distribution curve depicting a semilogarithmic dependence of cumulative pore volume on the pore diameter interval. The results are also interpretable as the dependence of pore occurrence per the interval of their diameter. The maximum of the curve corresponds to the most frequent pore diameter.

All these principles are based on the estimation that the structure of the sample is rigid and during experiment does not change. There is no deformation or compression of the sample by mercury during enhancing of the pressure in the apparatus cell. Nanofibrous nonwoven fabrics are constructed of single fibers of small diameter and relatively large free volume among these fibers. Unlike other materials, internal structure of nanofibrous materials can be changed easily even under low pressure of mercury. The fibers are deformed, they change their shape and location and the size and volume of the pores among fibers change as well. Therefore, the size and volume of the pores found by mercury porosimetry may be to a certain extant misguided. However, mercury porosimetry has an important role in characterization of nanofibers.

Mercury under the pressure from 100 kPa to 207 MPa was applied during the porosimetry measurements on fibers prepared from various ratios of poly(L-lactide) and poly(ε-caprolactone) [40]. Total porosities (56–63%) were slightly lower than the values calculated from density of fabrics and density of the polymer (69–76%). The difference in the fiber diameter led to the difference in the fabric density—the densest fabric was found to be fabric with smallest fiber diameters (mean diameter 0.32 μm). Total pore volume of this fabric as well as mean pore radius was in this case the lowest. Pore size distribution curve had maximum at the smaller-pore region (0.1–10 μm). On the other hand, fabric from the thickest fibers (mean diameter 7.02 μm) exhibited almost no pores in this region; the maximum of the pore sizes was in the large-pore region. Fabric consisted of the fibers with mean diameter 1.16 μm exhibited bimodal pore distribution character. Mechanical properties as well as results of biological experiments are furthermore discussed. Consequence of porosity investigation results with cell cultivation outgrowth has been also described by Lowery et al. [55]. Porosity of inorganic nanofibers was explored by Ko et al. [56]. Ryu et al. [24] investigated influence of the electrospinning conditions on the structure of nylon nanofibers. Determination of fiber diameters by SEM was supplemented by pore size distribution curves obtained from mercury porosimetry measurements. The total pore volume ranged from 25% to 80%. With increasing polymer concentration (electrospinning process parameter), the average pore sizes increased as well as fiber diameters. This was followed by wider pore size distributions. As expected, with increasing fiber diameter the specific surface areas decreased.

2.3. BET Surface Area Measurements. The technique named after its inventors Brunauer, Emmett and Teller (BET) [57] is the most frequent method for determination of specific surface area of porous materials. The measurement is based on physical adsorption of gas on the sample surface. The amount of gas can be defined by the Langmuir isotherm assuming a monolayer of gas molecules on the homogenous surface which are not mutually affected.

$$a = \frac{qKp}{(1+Kp)}, \tag{2}$$

where a is the amount of gas adsorbed in 1 g of sample (mol/g), q is the amount of active centers in 1 g of sample (mol/g), p is partial pressure of the gas, and K is equilibrium coefficient of adsorption.

For a sample covered by gas molecules in more than one layer, the BET isotherm is applicable:

$$\frac{p}{p_0} = \frac{1}{a_m C} + \frac{p_0(C-1)}{a_m C}, \tag{3}$$

where p_0 is tension of saturated vapor at particular temperature, a_m is the amount of gas adsorbed in 1 g of sample in a monolayer (mol/g), and C is a constant including adsorption and condensation heat.

The adsorption isotherm depicts the dependence of the amount of adsorbed gas on the pressure at constant temperature. From isotherm measurements, the specific surface area is determined according to

$$A_{SP} = N_A \cdot a_m \cdot \sigma, \tag{4}$$

where A_{SP} is the specific surface area, N_A is the Avogadro constant, and σ is the area of the sample covered by one molecule of the adsorbing gas.

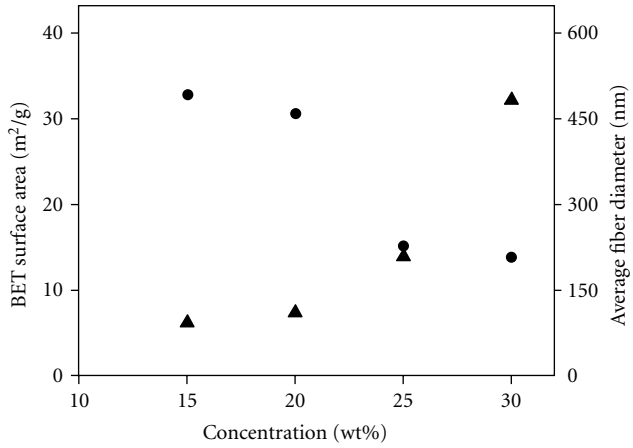

Figure 6: BET surface areas and average fiber diameters of electrospun nylon nanofibers as a function of polymer concentration (• BET surface area, ▲ average fiber diameter) [24].

The determined values of specific surface area are dependent on the used adsorbing gas—lower values are obtained with larger molecules. Usually nitrogen or argon is used.

BET method was used for determination of specific surface areas of nanofibers or for observation of changes that appear in the structure during postpreparation modification of inorganic [58] as well as organic nanofibers [59]. Important information brought BET in characterization of nanofibers with internal porosity [60] or in investigation of the influence of preparation conditions on the subsequent structure of nanofibers [24]. The relationship of specific surface area and average fiber diameter as a function of polymer concentration is shown in Figure 6.

Another method used for determination of specific surface area is adsorption of a chemical compound from an organic solvent or adsorption of isotopically labelled compound. Since the molecules of these compounds are usually considerably larger, they do not get into the smallest pores and the measured values are lower compared with those obtained using the BET technique.

Since mercury porosimetry can bring misleading results due to the mechanical deformation of the nanofibers [24, 61] and BET measurements bring only specific surface area value and distribution of pores up to 10 nm in diameter, a simple experiment based on liquid absorption can be used to measure the total pore volume. If the swelling of the fibers is practically negligible, then the amount of water (or any other liquid in which nanofibers do not swell) retained in the sample expresses the total pore volume.

2.4. Contact Angle Measurements. Besides the morphology and mechanical properties an important attribute for materials applicable in tissue engineering is their chemical composition. In the development of new scaffold the optimization of its surface properties with regard to the particular application is the critical step. The hydrophilic/hydrophobic character of the surface substantially influenced the interaction between the synthetic surface and living tissue.

To determine the degree of hydrophilicity of the given surface, contact angle measurement is the most spread method. The measurement is done using a sessile drop or captive bubble technique in static or dynamic mode. General aspects of contact angle measurements and interface energetics were described in detail for example by Andrade [62].

It is often not considered that the measurement of contact angle is not influenced only by chemical composition of the sample, but also by the surface structure, heterogeneities, and other factors. The effect of the surface roughness has been explained by Wenzel [63] (lower degrees of roughness) and Cassie and Baxter [64] (higher degrees of roughness) model. According to the Wenzel model, larger surface area and subsequently larger interfacial energy of water-solid interface induces penetration of water to the surface cavities. In the case of higher degrees of surface roughness (Cassie-Baxter model), water droplets contact air pockets between water and rough solid surface, but do not penetrate into the cavities. In both cases, measured contact angle may be different from the result obtained for the same material but with smooth surface.

Taniguchi et al. investigated influence of the surface roughness on the results of contact angle measurement in detail. Poly(ether sulfone) membranes with different pore size were prepared as the model of rough porous surfaces of the same surface chemistry. Using AFM he proposed roughness parameters for correction of the results obtained by captive bubble/drop measurement [65]. Similar corrections have been adapted for measurement of advancing and receding contact angles in dynamic mode [66].

It is clear that contact angle measurements on nanofibrous materials representing porous, deformable solids, eventually swelling in water, must be taken with caution.

However, a number of studies have focused on evaluation of the changes in hydrophilicity of the nanofibers after a surface modification using contact angle measurements [67]. The use of plasma [35, 36], in some cases, accompanied by immobilization of bioactive compounds [34, 68] and the subsequent influence of surface treatment on cellular response was described.

3. Part 2—Experimental Part: Morphological Characterization of Electrospunned Nanofibers

We prepared various nanofibers by electrospinning using laboratory Nanospider apparatus (Elmarco, Czech Republic) (Figure 7). A thin layer of polymer solution film (b) is raised by a metal roller (rotating spinning electrode) (a), which is at the same time the positive electrode. This electrode is partially submerged in the polymer solution (c) and nanofibers are created between spinning electrode and collector due to very high intensity electrostatic field (20–45 kV/cm) by force of Taylor's cones (e). After solvent evaporation, the fibers stretch at room or elevated temperature are collected by

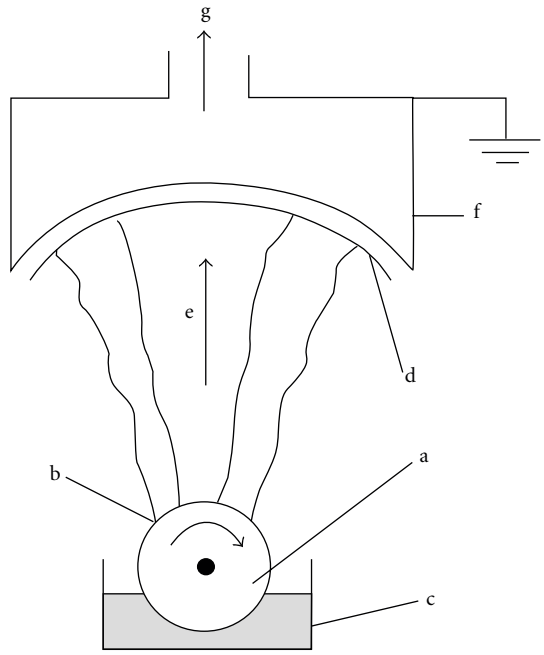

Figure 7: Principle of electrospinning: (a) electrode metal roller as positive electrode, (b) fiberforming polymer layer, (c) reservoir of polymer solution, (d) textile substrate (supportive material), (e) fiber formation direction, (f) electrode earthing shield, (g) air suction.

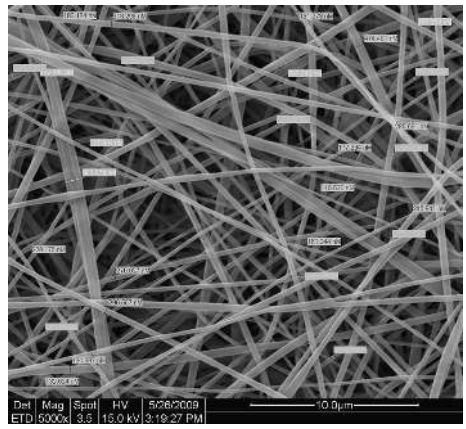

Figure 8: SEM image of polyamide nanofibers with an illustrative example of determination of the average fiber diameter.

a nonwoven fabric (d) on the negative electrode (f). Polymers polylactide (PLA), poly(ε-caprolactone) (PCL), gelatin, and polyamide (PA) were used to prepare nanofibers. Mean diameter of fibers was between 100 and 400 nm. Thickness (area weight) was between 3 and 50 g/m^2.

The structure of prepared nanofibers was observed by scanning electron microscope TS 5130 VEGA, TESCAN (Czech Republic). The fiber diameters were determined as mean values of 30 measurements on the SEM images at 5000x magnification as it is illustrated on Figure 8 and values are summarized in Table 1. Apparently, the thinnest fibers were obtained in the case of gelatin (mean value 110 nm), in the case of other polymers the mean values were between 160 and 390 nm.

In some cases, heterogeneities or artifacts were found. Nanofibers prepared from PLA under given electrospinning conditions were characterised by bunches of fibers with higher density among which the structure was tenuous with larger pores (Figure 9(a)). Primary optimization of electrospinning conditions brought nanofibrous structure composed of layers of fibers with higher density; space between layers was more porous again (Figure 9(b)). Another optimization of electrospinning brought nanofibrous nonwovens with homogenous structures, required for biological or medicinal applications.

Similar case was observed in the preparation of nanofibers from PCL; during electrospinning the artifacts in the fibrous structures appeared. Large amount of material was in these formations (Figures 9(c) and 9(d)). Subsequent modification of electrospinning process precluded the creation of these artifacts and homogenous structure of PCL nanofibers was achieved.

SEM method enables to reveal appearance of heterogeneities in the structure that may have significant impact on behavior of nanofibrous materials in medicinal applications, that is, cell cultivation or drug release.

In some medicinal applications such as cultivation of cells for nervous tissue reparation, orientation of supporting nanofibrous nonwoven has significant effect on the cell growth, formation, and orientation. SEM images of PA, PLA, and gelatin nanofibers with random and parallel orientation are depicted on Figure 10 and supplemented by images from confocal microscope depicting the cultivation of mesenchymal stem cells. Apparently, the shape of cell changed and they followed the fiber orientation.

Mercury porosimetry measurements were made using an Autopore IV 9500 porosimeter (Micromeritics, USA). The measurement had two parts. There were two low pressure ports where the analysis took place. The evacuation of sample and low pressure measurement run from 0.01 MPa to 0.25 MPa, under these conditions the pores with radius from 100 μm to 3 μm approximately were analyzed. The high pressure chamber was used for high pressure analysis from 0.25 MPa to 400 MPa. It covered the range of pore radius from 3 μm to 1.5 nm. The nanofibers of various thicknesses (area weight) made from PLA, PCL, gelatin, and PA were examined. The mercury intrusion/extrusion curves for PLA samples of 3.5, 8.7, 12.6 g/m^2 and PA samples of 3.3 g/m^2 are shown in Figure 11. The curves of samples of various thickness made from PLA were found to be very similar. According to the shape of the curve the mercury was intruded into the space between nanofibers. In the case of PA nanofibers with thickness 3.3 g/m^2, the larger space between the fibers was observed and also higher porosity was measured (84.8%, see Table 1, column Porosity).

Pore size distribution curves of PLA nanofibers are shown in Figure 12. Local maximum of the curve, which represents the most frequent pore diameter, was found around 0.6 μm. Due to the shape of the distribution curve,

Table 1: Morphological characterization of nanofibres.

Polymer	Area weight g/m^2	Absorption capacity[a]	Absorption capacity[b]	Porosity %	Specific surface area m^2/g	Average fiber diameter nm
PLA	3.5	92.3	11.3	77.1	6	
PLA	4.2	90.3	9.6	—	—	
PLA	8.7	87.8	7.2	65.2	7.5	390
PLA	9.7	84.9	5.6	—	—	
PLA	12.6	83.2	5	61.8	6.2	
PCL	3.4	98.2	60.3	62.2	7.3	160
PCL	10	87	6.7	—	—	
Gelatin	4.5	95.4	20.8	84.8	17.6	110
Gelatin	50	93.5	10.2	86.9	16.6	
PA	3.3	97.5	41.7	84.8	7.3	280
PA	57.8	76.2	3.2	—	—	

[a]Absorption capacity of nanofibers calculated as $(m_W - m_D)/m_W$ where m_W is mass of wet nanofibers and m_D is mass of dry nanofibers.
[b]Absorption capacity of nanofibers expressed as (m_{H_2O}/m_D) where m_{H_2O} is mass of water absorbed by nanofibers and m_D is mass of dry nanofibers.

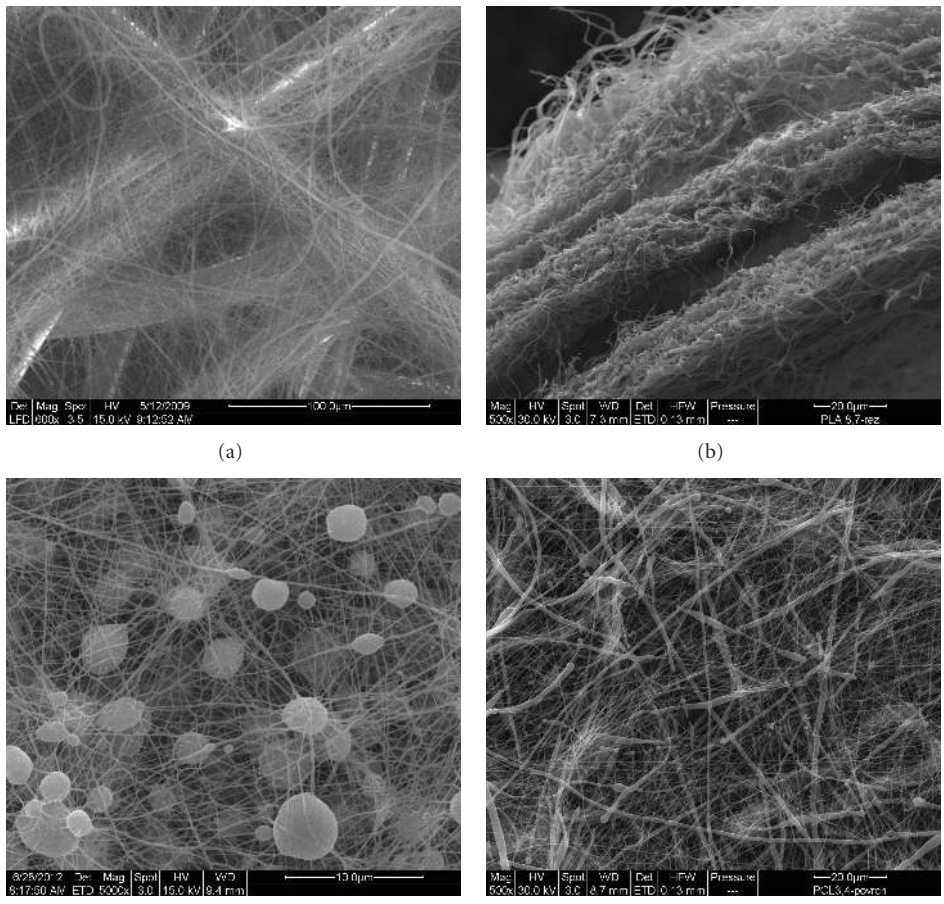

Figure 9: SEM images depicting heterogeneities in polylactide nanofibrous structures (a), (b) and artifacts in poly(ε-caprolactone) nanofibrous samples (c), (d).

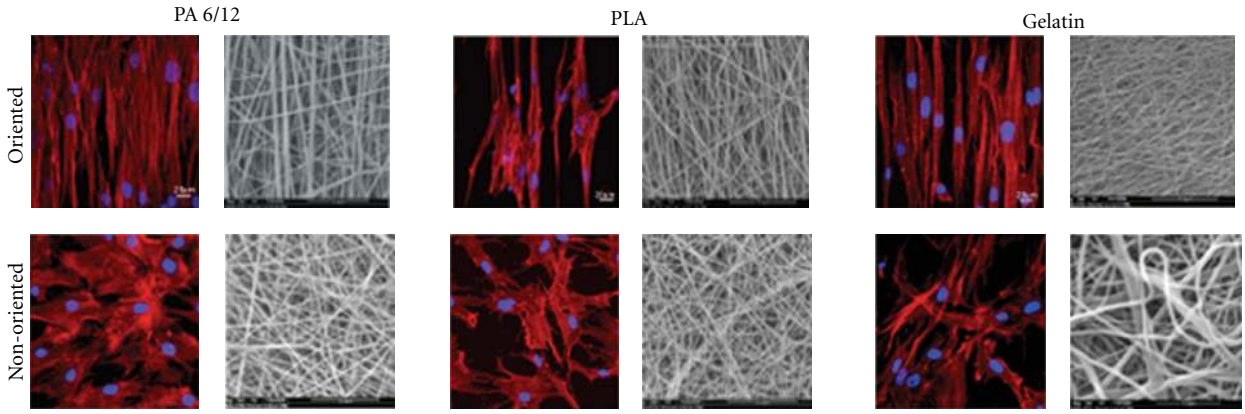

Figure 10: Images of mesenchymal stem cells (obtained by confocal microscope LSM 510 DUO, Zeiss) grown on the nanofibers with parallel and random orientation (images from scanning electron microscope TS 5130 VEGA, Tescan).

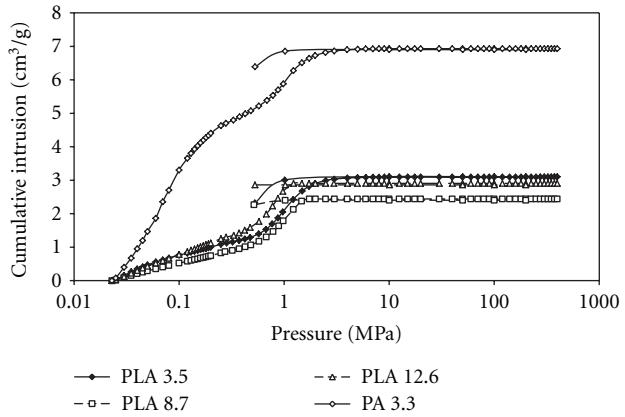

Figure 11: Intrusion and extrusion curves measured by mercury porosimetry on polylactide nanofibers of 3.5, 8.7, and 12.6 g/m^2 and polyamide nanofibers of 3.3 g/m^2 area weight.

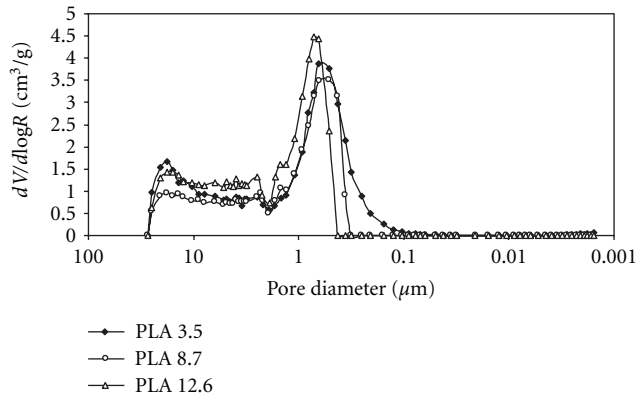

Figure 12: Pore size distribution curves of polylactide nanofibers of 3.5, 8.7, and 12.6 g/m^2 area weight.

also the median pore size was close to this value (PLA 3.6–0.5 μm, PLA 8.7–0.5 μm, PLA 12.6–0.7 μm). Total pore volume decreased with increasing sample thickness (see Table 1, column Porosity). Different shape of the distribution curves was found for gelatin samples of 4.5 and 50 g/m^2 (Figure 13). The distributions were broad with small local maxima. Also no significant difference between samples of various thicknesses was seen. Total porosities were 84.8 and 86.9 %.

The values of pore diameter occurrence in the range 0.01–0.001 μm suggest that all the observed nanofibrous samples exhibited almost no pores inside the single fibers. All the found pore volume belongs to the interspaces between the fibers. This property also corresponds to the SEM findings.

Since mercury porosimetry may be significantly influenced by the mechanical properties of the nanofibers [24, 61], a simple experiment was used to compare the total pore volumes of individual samples. The absorption capacity was taken as an approximation of pore volume. If the swelling of the fibers is practically negligible, then the amount of liquid (in our case water) retained in the sample expresses the total pore volume. The samples of nanofibers were removed from the support textile, dried, weighed, and soaked into the distilled water at laboratory temperature. After 12 hours the samples were removed, kept in an upright position for 30 s to drop the remaining water out and weighed again. The volume of water corresponds to the total volume of the pores in the sample. Absorption capacity was expressed as the ratio of the weight of retained water (m_{H_2O}) per dry polymer weight (m_D) or calculated in percentage as $(m_W - m_D)/m_W$ where m_W is mass of wet nanofibers and m_D is mass of dry nanofibers. Similarly, weighing the dried samples (e.g., by filtration paper) it is possible to calculate the amount of retained water caused by fiber swelling or loss of mass caused by fiber degradation. In our experiment, fibers were made from polymers that do not swell significantly and also their degradation was negligible. This very simple measurement can bring representative results of total pore volume. Even small difference among various samples can be revealed as it is apparent from Table 1. When the samples of similar area weight were compared, the greatest absorption capacity was found for PCL nanofibers (60.3).

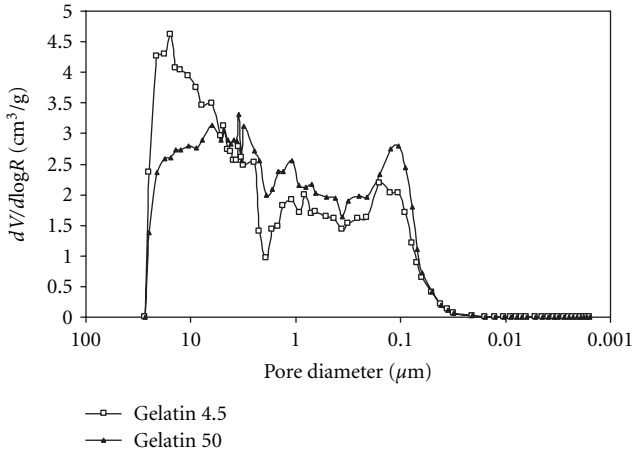

Figure 13: Pore size distribution curves of gelatin nanofibers of 4.5 and 50.0 g/m^2 area weight.

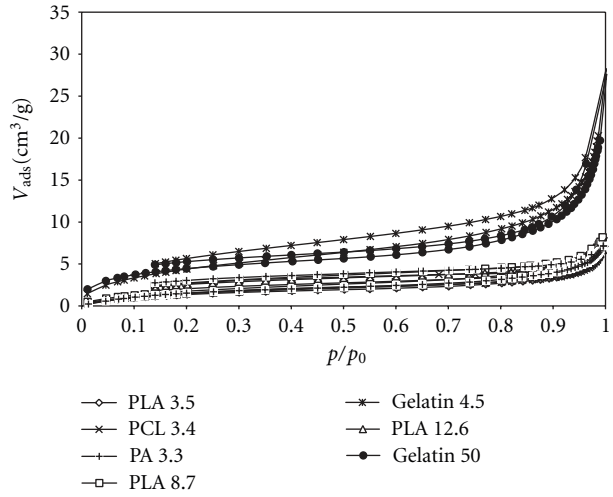

Figure 14: Equilibrium nitrogen adsorption isotherms of polylactide, poly(ε-caprolactone), gelatin, and polyamide of various area weights.

On the other hand, the lowest capacity was found for PLA nanofibers (11.3). When the samples of PLA of various thicknesses were compared, close relationship appeared. Sample of 3.5 g/m^2 absorbed 11.3 while the thickest sample (12.6 g/m^2) absorbed only 5.0. The same relationship was obvious from the values of total porosities measured by mercury porosimetry. The trend in decreasing the total pore volume with increasing sample thickness can be explained by the formation of more compressed structure during the preparation.

The specific surface areas were calculated from nitrogen absorption/desorption isotherms recorded on the apparatus ASAP 2020 (Micromeritics, USA). The adsorption isotherms measured on the selected nanofibrous samples revealed almost similar specific surface areas (BET) between 6 and 8 m^2/g for PLA, PCL, and PA (see Table 1). Significantly higher specific surface area about 17 m^2/g was found in case of gelatin nanofibers. This value, different from the others, was probably caused by the lowest average nanofiber diameter and not strictly cylindrical shape of the nanofibers.

Materials of various structures provide various values and shapes of gas adsorption and desorption isotherms. Courses of the measured isotherms (Figure 14), together with relatively low specific surface areas (Table 1), predict about low amount of micropores and mesopores. Therefore, it can be presumed that all tested samples exhibited very low or almost imperceptible porosity inside the fibers. These results also correspond to the pore size distribution curves that were calculated by BJH method (Figure 15). Slightly higher porosities in case of gelatin nanofibers compared to the others, together with higher specific surface areas correspond to the thinner diameters and rugged surface of these nanofibers.

In summary, microscopy techniques, mercury porosimetry, nitrogen adsorption/desorption BET measurement as well as simple soaking experiment bring valuable results, however, each method has some disadvantages and limitations.

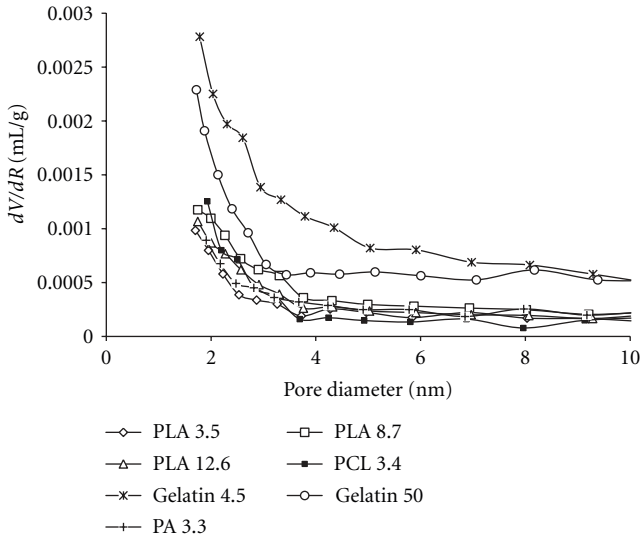

Figure 15: Pore size distribution curves in the range of 1.6 to 10 nm calculated from adsorption/desorption isotherms by BJH method.

4. Summary

Needleless electrospinning was used to prepare nanofibers from polylactide, poly(ε-caprolactone), gelatin, and polyamide. The preparation process was optimized and nanofibrous nonwoven textiles with homogenous structures and various area weights were prepared.

Scanning electron microscopy was used to observe the samples, to evaluate the fiber diameters, and to reveal eventual artifacts in the nanofibrous structure. Generally, it is an essential technique for observation of nanofibrous structures. In our experiment, the fiber diameters determined by SEM differed among nanofibers prepared from various polymers but they were not influenced by the sample

thickness. The measurements of pore size distributions by mercury porosimetry were significantly influenced by mechanical limitations of the nanofibrous samples, which most probably negatively affected the obtained absolute values. However, mercury porosimetry was found to be a crucial method for comparison of pore characters of samples among themselves. Experiments based on the soaking of nanofibers into the nonswelling liquid may be used for determination of total pore volumes. This simple method revealed small differences between nanofibrous samples. Both these techniques are usable for comparison of various samples; however, result of single method can be misguided. BET nitrogen adsorption/desorption measurements can be efficiently employed for specific surface area measurement, calculated distribution of pores with diameter 1.6–10 nm may bring valuable results about internal porosity of nanofibers.

According to the found results, it can be concluded that behavior of nanofibers during the morphological characterization is specific and significantly different compared to the rigid porous polymers. Therefore, the morphological characterization of nanofibrous materials requires a complex approach and evaluation of the results of various methods.

Acknowledgments

This work was supported by Grants AS CR KAN200520804 and GA CR 304/07/1129 and Ministry of Education, Youth and Sports of the Czech Republic, Grant CZ.1.07/2.3.00/30.0029.

References

[1] N. Bhardwaj and S. C. Kundu, "Electrospinning: a fascinating fiber fabrication technique," *Biotechnology Advances*, vol. 28, no. 3, pp. 325–347, 2010.

[2] I. Ahmed, A. S. Ponery, E. K. A. Nur et al., "Morphology, cytoskeletal organization, and myosin dynamics of mouse embryonic fibroblasts cultured on nanofibrillar surfaces," *Molecular and Cellular Biochemistry*, vol. 301, no. 1-2, pp. 241–249, 2007.

[3] Y. R. V. Shih, C. N. Chen, S. W. Tsai, J. W. Yng, and O. K. Lee, "Growth of mesenchymal stem cells on electrospun type I collagen nanofibers," *Stem Cells*, vol. 24, no. 11, pp. 2391–2397, 2006.

[4] E. J. Chong, T. T. Phan, I. J. Lim et al., "Evaluation of electrospun PCL/gelatin nanofibrous scaffold for wound healing and layered dermal reconstitution," *Acta Biomaterialia*, vol. 3, no. 3, pp. 321–330, 2007.

[5] M. Hadjiargyrou and J. B. Chiu, "Enhanced composite electrospun nanofiber scaffolds for use in drug delivery," *Expert Opinion on Drug Delivery*, vol. 5, no. 10, pp. 1093–1106, 2008.

[6] Z. G. Wang, L. S. Wan, Z. M. Liu, X. J. Huang, and Z. K. Xu, "Enzyme immobilization on electrospun polymer nanofibers: an overview," *Journal of Molecular Catalysis B*, vol. 56, pp. 189–195, 2009.

[7] X. B. Fu and H. H. Li, "Mesenchymal stem cells and skin wound repair and regeneration: possibilities and questions," *Cell and Tissue Research*, vol. 335, no. 2, pp. 317–321, 2009.

[8] G. Pellegrini, P. Rama, F. Mavilio, and M. de Luca, "Epithelial stem cells in corneal regeneration and epidermal gene therapy," *Journal of Pathology*, vol. 217, no. 2, pp. 217–228, 2009.

[9] X. B. Xing, Y. Q. Wang, and B. J. Li, "Nanofiber drawing and nanodevice assembly in poly(trimethylene terephthalate)," *Optics Express*, vol. 16, no. 14, pp. 10815–10822, 2008.

[10] K. L. Niece, J. D. Hartgerink, J. J. J. M. Donners, and S. I. Stupp, "Self-assembly combining two bioactive peptide-amphiphile molecules into nanofibers by electrostatic attraction," *Journal of the American Chemical Society*, vol. 125, no. 24, pp. 7146–7147, 2003.

[11] Z. M. Huang, Y. Z. Zhang, M. Kotaki, and S. Ramakrishna, "A review on polymer nanofibers by electrospinning and their applications in nanocomposites," *Composites Science and Technology*, vol. 63, pp. 2223–2253, 2003.

[12] A. Martins and R. L. Reis, "Electrospinning: processing technique for tissue engineering scaffolding," *International Materials Reviews*, vol. 53, pp. 257–274, 2008.

[13] C. J. Luo, S. D. Stoyanov, E. Stride, E. Pelan, and M. Edirisinghe, "Electrospinning versus fibre production methods: from specifics to technological convergence," *Chemical Society Reviews*, vol. 41, pp. 4708–4735, 2012.

[14] P. R. Kumar, N. Khan, S. Vivekanandhan, N. Satyanarayana, A. K. Mohanty, and M. Misra, "Nanofibers: effective generation by electrospinning and their applications ," *Journal of Nanoscience and Nanotechnology*, vol. 12, pp. 1–25, 2012.

[15] G. H. Lee, J. C. Song, and K. B. Yoon, "Controlled wall thickness and porosity of polymeric hollow nanofibers by coaxial electrospinning," *Macromolecular Research*, vol. 18, pp. 571–576, 2010.

[16] C. Wang, K. W. Yan, Y. D. Lin, and P. C. H. Hsieh, "Biodegradable core/shell fibers by coaxial electrospinning: processing, fiber characterization, and its application in sustained drug release," *Macromolecules*, vol. 43, no. 15, pp. 6389–6397, 2010.

[17] M. Kamperman, L. T. J. Korley, B. Yau, K. M. Johansen, Y. L. Joo, and U. Wiesner, "Nanomanufacturing of continuous composite nanofibers with confinement-induced morphologies," *Polymer Chemistry*, vol. 1, no. 7, pp. 1001–1004, 2010.

[18] S. L. Chen, H. Q. Hou, P. Hu, J. H. Wendorff, A. Greiner, and S. Agarwal, "Polymeric nanosprings by bicomponent electrospinning," *Macromolecular Materials and Engineering*, vol. 294, no. 4, pp. 265–271, 2009.

[19] S. L. Chen, H. Q. Hou, P. Hu, J. H. Wendorff, A. Greiner, and S. Agarwal, "Effect of different bicomponent electrospinning techniques on the formation of polymeric nanosprings," *Macromolecular Materials and Engineering*, vol. 294, no. 11, pp. 781–786, 2009.

[20] G. F. Taylor, "Electrically driven jets," *Proceedings of the Royal Society of London A*, vol. 313, pp. 453–475, 1969.

[21] J. C. Park, "Electric spinning apparatus for mass-production of nano-fiber," U.S. Patent, 2008.

[22] O. Jirsak, F. Sanetrnik, D. Lukas, L. Kotek, L. Martinova, and J. Chaloupek, "Method of nanofibers production from polymer solution using electrostatic spinning and a device for carrying out the method," U.S. Patent, WO, 20060290031, 2006.

[23] D. Lukas, A. Sarkar, and P. Pokorny, "Self-organization of jets in electrospinning from free liquid surface: a generalized approach ," *Journal of Applied Physics*, vol. 103, no. 8, Article ID 084309, 2008.

[24] Y. J. Ryu, H. Y. Kim, K. H. Lee, H. C. Park, and D. R. Lee, "Transport properties of electrospun nylon 6 nonwoven mats," *European Polymer Journal*, vol. 39, no. 9, pp. 1883–1889, 2003.

[25] C. P. Barnes, S. A. Sell, E. D. Boland, D. G. Simpson, and G. L. Bowlin, "Nanofiber technology: designing the next

generation of tissue engineering scaffolds," *Advanced Drug Delivery Reviews*, vol. 59, no. 14, pp. 1413–1433, 2007.

[26] R. Chen, C. Huang, Q. F. Ke, C. L. He, H. S. Wang, and X. M. Mo, "Preparation and characterization of coaxial electrospun thermoplastic polyurethane/collagen compound nanofibers for tissue engineering applications," *Colloids and Surfaces B*, vol. 79, no. 2, pp. 315–325, 2010.

[27] Y. Srivastava, M. Marquez, and T. Thorsen, "Microfluidic electrospinning of biphasic nanofibers with Janus morphology," *Biomicrofluidics*, vol. 3, no. 1, Article ID 012801, 2009.

[28] K. H. Lee, H. Y. Kim, Y. J. Ryu, K. W. Kim, and S. W. Choi, "Mechanical behavior of electrospun fiber mats of poly(vinyl chloride)/polyurethane polyblends," *Journal of Polymer Science B*, vol. 41, no. 11, pp. 1256–1262, 2003.

[29] M. Forouharshad, O. Saligheh, R. Arasteh, and R. E. Farsani, "Manufacture and characterization of poly (butylene terephthalate) nanofibers by electrospinning," *Journal of Macromolecular Science B*, vol. 49, no. 4, pp. 833–842, 2010.

[30] L. M. Guerrini, M. P. de Oliveira, M. C. Branciforti, T. A. Custodio, and R. E. S. Bretas, "Thermal and structural characterization of nanofibers of poly(vinyl alcohol) produced by electrospinning," *Journal of Applied Polymer Science*, vol. 112, pp. 1680–1687, 2009.

[31] Z. Q. Peng, Y. Yoshida, and S. Sukigara, "Morphology and physical properties of a novel ramie-PU blended nonwoven by electrospinning: the effect of cosolvent ratio," *Journal of Polymer Science B*, vol. 48, no. 1, pp. 1–14, 2010.

[32] J. H. Park, H. W. Lee, D. K. Chae et al., "Electrospinning and characterization of poly(vinyl alcohol)/chitosan oligosaccharide/clay nanocomposite nanofibers in aqueous solutions," *Colloid and Polymer Science*, vol. 287, no. 8, pp. 943–950, 2009.

[33] J. M. Lim, G. R. Yi, J. H. Moon, C. J. Heo, and S. M. Yang, "Superhydrophobic films of electrospun fibers with multiple-scale surface morphology," *Langmuir*, vol. 23, no. 15, pp. 7981–7989, 2007.

[34] I. Shabani, V. Haddadi-Asl, E. Seyedjafari, F. Babaeijandaghi, and M. Soleimani, "Improved infiltration of stem cells on electrospun nanofibers," *Biochemical and Biophysical Research Communications*, vol. 382, no. 1, pp. 129–133, 2009.

[35] A. Martins, E. D. Pinho, S. Faria et al., "Surface modification of electrospun polycaprolactone nanofiber meshes by plasma treatment to enhance biological performance," *Small*, vol. 5, no. 10, pp. 1195–1206, 2009.

[36] K. E. Park, K. Z. Lee, S. J. Lee, and W. H. Park, "Surface characteristics of plasma-treated PLGA nanofibers," *Macromolecular Symposia*, vol. 249-250, pp. 103–108, 2007.

[37] S. J. Kim, D. H. Jang, W. H. Park, and B. M. Min, "Fabrication and characterization of 3-dimensional PLGA nanofiber/microfiber composite scaffolds," *Polymer*, vol. 51, no. 6, pp. 1320–1327, 2010.

[38] C. B. Huang, S. L. Chen, D. H. Reneker, C. L. Lai, and H. Q. Hou, "High-strength mats from electrospun poly(*p*-phenylene biphenyltetracarboximide) nanofibers," *Advanced Materials*, vol. 18, pp. 668–671, 2006.

[39] S. L. Chen, P. Hu, A. Greiner et al., "Electrospun nanofiber belts made from high performance copolyimide," *Nanotechnology*, vol. 19, no. 1, Article ID 015604, 2008.

[40] I. K. Kwon, S. Kidoaki, and T. Matsuda, "Electrospun nano- to microfiber fabrics made of biodegradable copolyesters: structural characteristics, mechanical properties and cell adhesion potential," *Biomaterials*, vol. 26, no. 18, pp. 3929–3939, 2005.

[41] N. Amiraliyan, M. Nouri, and M. H. Kish, "Electrospinning of silk nanofibers. I. An investigation of nanofiber morphology and process optimization using response surface methodology," *Fibers and Polymers*, vol. 10, no. 2, pp. 167–176, 2009.

[42] D. H. Reneker, W. Kataphinan, A. Theron, E. Zussman, and A. L. Yarin, "Nanofiber garlands of polycaprolactone by electrospinning," *Polymer*, vol. 43, no. 25, pp. 6785–6794, 2002.

[43] V. Jacobs, R. D. Anandjiwala, and M. Maaza, "The influence of electrospinning parameters on the structural morphology and diameter of electrospun nanofibers," *Journal of Applied Polymer Science*, vol. 115, no. 5, pp. 3130–3136, 2010.

[44] N. Amiraliyan, M. Nouri, and M. H. Kish, "Effects of some electrospinning parameters on morphology of Natural silk-based nanofibers," *Journal of Applied Polymer Science*, vol. 113, no. 1, pp. 226–234, 2009.

[45] E. Tomba, P. Facco, M. Roso, M. Modesti, F. Bezzo, and M. Barolo, "Artificial vision system for the automatic measurement of interfiber pore characteristics and fiber diameter distribution in nanofiber assemblies," *Industrial and Engineering Chemistry Research*, vol. 49, no. 6, pp. 2957–2968, 2010.

[46] P. Facco, E. Tomba, M. Roso, M. Modesti, F. Bezzo, and M. Barolo, "Automatic characterization of nanofiber assemblies by image texture analysis," *Chemometrics and Intelligent Laboratory Systems*, vol. 103, no. 1, pp. 66–75, 2010.

[47] H. M. Ji, H. W. Lee, M. R. Karim et al., "Electrospinning and characterization of medium-molecular-weight poly(vinyl alcohol)/high-molecular-weight poly(vinyl alcohol)/ montmorillonite nanofibers," *Colloid and Polymer Science*, vol. 287, no. 7, pp. 751–758, 2009.

[48] C. Y. Cheng, J. Chen, F. Chen et al., "High-strength and high-toughness polyimide nanofibers: synthesis and characterization," *Journal of Applied Polymer Science*, vol. 116, no. 3, pp. 1581–1586, 2010.

[49] B. M. Min, G. Lee, S. H. Kim, Y. S. Nam, T. S. Lee, and W. H. Park, "Electrospinning of silk fibroin nanofibers and its effect on the adhesion and spreading of normal human keratinocytes and fibroblasts in vitro," *Biomaterials*, vol. 25, no. 7-8, pp. 1289–1297, 2004.

[50] H. Q. Cao, K. Mchugh, S. Y. Chew, and J. M. Anderson, "The topographical effect of electrospun nanofibrous scaffolds on the in vivo and in vitro foreign body reaction," *Journal of Biomedical Materials Research A*, vol. 93, pp. 1151–1159, 2010.

[51] U. Stachewicz and A. H. Barber, "Enhanced wetting behavior at electrospun polyamide nanofiber surfaces," *Langmuir*, vol. 27, no. 6, pp. 3024–3029, 2011.

[52] K. Y. Hwang, S. D. Kim, Y. W. Kim, and W. R. Yu, "Mechanical characterization of nanofibers using a nanomanipulator and atomic force microscope cantilever in a scanning electron microscope," *Polymer Testing*, vol. 29, no. 3, pp. 375–380, 2010.

[53] H. L. Ritter and L. C. Drake, "Pressure porosimeter and determination of complete macropore-size distributions. Pressure porosimeter and determination of complete macropore-size distributions," *Industrial and Engineering Chemistry Analytical Edition*, vol. 17, no. 12, pp. 782–786, 1945.

[54] E. W. Washburn, "Note on a method of determining the distribution of pore sizes in a porous material," *Proceedings of the National Academy of Sciences*, vol. 7, pp. 115–116, 1921.

[55] J. L. Lowery, N. Datta, and G. C. Rutledge, "Effect of fiber diameter, pore size and seeding method on growth of human dermal fibroblasts in electrospun poly(ε-caprolactone) fibrous mats," *Biomater*, vol. 31, pp. 491–504, 2010.

[56] J. B. Ko, S. W. Lee, D. E. Kim et al., "Fabrication of SiO_2-ZrO_2 composite fiber mats via electrospinning," *Journal of Porous Materials*, vol. 13, no. 3, pp. 325–330, 2006.

[57] S. Brunauer, P. H. Emmett, and E. J. Teller, "Adsorption of gases in multimolecular layers," *Journal of the American Chemical Society*, vol. 60, no. 2, pp. 309–319, 1938.

[58] A. M. Bazargan, S. M. A. Fateminia, M. E. Ganji, and M. A. Bahrevar, "Electrospinning preparation and characterization of cadmium oxide nanofibers," *Chemical Engineering Journal*, vol. 155, no. 1-2, pp. 523–527, 2009.

[59] S. Imaizumi, H. Matsumoto, K. Suzuki, M. Minagawa, M. Kimura, and A. Tanioka, "Phenolic resin-based carbon thin fibers prepared by electrospinning: additive effects of poly(vinyl butyral) and electrolytes," *Polymer Journal*, vol. 41, no. 12, pp. 1124–1128, 2009.

[60] Z. Y. Zhang, X. H. Li, C. H. Wang, S. W. Fu, Y. C. Liu, and C. L. Shao, "Polyacrylonitrile and carbon nanofibers with controllable nanoporous structures by electrospinning," *Macromolecular Materials and Engineering*, vol. 294, pp. 673–678, 2009.

[61] Q. P. Pham, U. Sharma, and A. G. Mikos, "Electrospun poly(ε-caprolactone) microfiber and multilayer nanofiber/microfiber scaffolds: characterization of scaffolds and measurement of cellular infiltration," *Biomacromolecules*, vol. 7, pp. 2796–2805, 2006.

[62] J. D. Andrade, *Surface and Interfacial Aspects of Biomedical Polymers*, Plenum Press, New York, NY, USA, 1985.

[63] R. N. Wenzel, "Resistance of solid surfaces to wetting by water," *Industrial and Engineering Chemistry*, vol. 28, pp. 988–994, 1936.

[64] A. B. D. Cassie and S. Baxter, "Wettability of porous surfaces," *Transactions of the Faraday Society*, vol. 40, pp. 546–551, 1944.

[65] M. Taniguchi, J. P. Pieracci, and G. Belfort, "Effect of undulations on surface energy: a quantitative assessment," *Langmuir*, vol. 17, no. 14, pp. 4312–4315, 2001.

[66] M. Taniguchi and G. Belfort, "Correcting for surface roughness: advancing and receding contact angles," *Langmuir*, vol. 18, no. 16, pp. 6465–6467, 2002.

[67] H. S. Yoo, T. G. Kim, and T. G. Park, "Surface-functionalized electrospun nanofibers for tissue engineering and drug delivery," *Advanced Drug Delivery Reviews*, vol. 61, pp. 1033–1042, 2009.

[68] J. Jia, Y. Y. Duan, J. Yu, and J. W. Lu J, "Preparation and immobilization of soluble eggshell membrane protein on the electrospun nanofibers to enhance cell adhesion and growth," *Journal of Biomedical Materials Research A*, vol. 86, pp. 364–373, 2008.